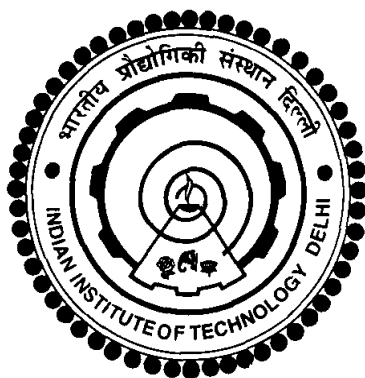


**INVESTIGATION OF NANOSTRUCTURED
METAL COBALTITES AND MANGANITES FOR
ELECTROCATALYTIC AND MAGNETIC
PROPERTIES**

NEHA GARG



**DEPARTMENT OF CHEMISTRY
INDIAN INSTITUTE OF TECHNOLOGY DELHI
INDIA
JANUARY 2016**

©Indian Institute of Technology Delhi (IITD), New Delhi, 2016

**INVESTIGATION OF NANOSTRUCTURED
METAL COBALTITES AND MANGANITES FOR
ELECTROCATALYTIC AND MAGNETIC
PROPERTIES**

by

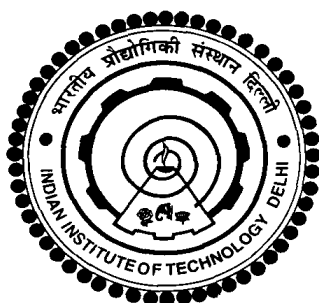
NEHA GARG

Department of Chemistry

Submitted in fulfillment of the requirements of the Degree of

Doctor of Philosophy

to the



INDIAN INSTITUTE OF TECHNOLOGY DELHI

INDIA

January 2016

Dedicated to
My Parents and My Husband

CERTIFICATE

This is to certify that the thesis entitled, “**Investigation of nanostructured metal cobaltites and manganites for electrocatalytic and magnetic properties**”, being submitted by **Mrs. Neha Garg**, to the Indian Institute of Technology, Delhi for the award of the degree of **Doctor of Philosophy** in Chemistry, is a record of bonafide research work carried out by her. Mrs. Neha Garg has worked under my guidance and supervision, and has fulfilled the requirements for the submission of this thesis, which to my knowledge has reached the requisite standard.

The results contained in this dissertation have not been submitted in part or full, to any other university or institute for award of any degree or diploma.

Date:

Prof. A. K. Ganguli

Department of Chemistry

Indian Institute of Technology, Delhi

New Delhi-110016

INDIA

Acknowledgements

I would like to thank lord '*Ganesha and My parents*' for giving me strength and blessings to complete this task successfully, I was eagerly waiting for. Completion of this doctoral thesis would not have possible without the support and devotions of those people coming across these hardship. I would like to express my sincere gratitude to all of them.

First and foremost, I would like to express my sincere regards and heartfelt gratitude to my Ph.D supervisor, **Prof. A. K. Ganguli** for giving me an opportunity to work under his guidance. I am really grateful for his valuable guidance, suggestions, scientific discussions, consistent encouragements and critical comments during the period of my research. He has always made himself available to clarify my doubts which helped me to learn a lot from his research expertise. I consider myself privileged for the opportunity to pursue my doctoral program under his guidance. His passion for science inspired me to do good research. Also I learnt from him the importance of punctuality and to tackle the difficulties by proper management and hard work. Working with him has been a wonderful learning experience.

I wish to express my sincere thanks to the Head of Chemistry Department, Prof. A. Ramanan and former Heads Prof. A. K. Singh, Department of Chemistry, IIT Delhi for providing me necessary facilities in the department. I would like to thank Dr. Pramit K. Chowdhury, Dr. Pravin P. Ingole, IIT Delhi Department of Chemistry, for their valuable suggestions and scientific discussions. I am grateful to them for their support and encouragement during my Ph.D. tenure. I owe thanks to all my teachers of department of Chemistry, IIT Delhi. I am also grateful to all the staff members of the department for

their cooperation and help. I am too grateful to Physics department, IIT Delhi for providing me SQUID facility for magnetic measurements.

I am extremely thankful to Prof. Ramanujachary and Prof. Lofland, Rowan University, U.S.A. for their help with the magnetic measurements. I would like to thank Dr. Hristo Kolev (Institute of Catalysis, Bulgarian Academy of Science) and Dr. Govind (National Physical Laboratory) for their help in the XPS measurements. I wish to convey my thanks to Dr. T. Prem Kumar and his student Dr. Sri Devi at CECRI, Karaikudi for their help in carrying out Li-ion battery experiments.

I express my sincere thanks to my lab-colleagues, former and present, especially Dr. Sonalika, Dr. Jahangeer, Dr. Aparna, Dr. Jai Prakash, Dr. Menaka, Dr. Aditya, Dr. Ashima, Dr. Mrinmoyee Basu, Dr. Masood Nath, Dr. Sharmila, Dr. R. Parthasarathy, Dr. Kanagaraj, Dr. Manu Sharma, Dr. Debashree, Dr. Sunita, Dr. Soma, Dr. Anjaniyulu, Bharat, Arabinda, Nibedita, Gohil, Soumen, Kasinath, Zeba, Vaishali, Sandeep, Nitin, Vandana for their love, understanding and providing an excellent working environment.

I am hearty grateful to my husband (Dr. Pramod Kumar) for his constant support, motivation, inspiration, understanding and love helped me a lot to complete my research. He always stood by my side in tough times, providing me strength and courage to handle the situations.

There are shortage of words to express my heartfelt thanks to my siblings, my loving sister Rimpal and a younger brother Ishu who always cheered me to solve every problem. I am heartily grateful to my sister in laws (Priti, Babita, Manju and Kumkum), brother in laws (Abhay Kesari, Anuj Kesari and Vinay), my nephew and nieces (Gopal,

Rishi, Divyansh, Varsha, Laado and Choti) for their love and support during my Ph.D. I am thankful to my whole family as during my research period everybody helped me at their best so that I could concentrate on my research work.

I owe everything to my parents- my mother (Smt. Sadhana Garg) and father (Sh. Subhash Chandra Garg). I could able to stand here for their all great sacrifices. Their struggle has made me reach this stage. I found them always standing by my side and supporting my decisions. Their love, inspiration and moral support was always there whenever I needed the most. They have been a constant source of encouragement and strength. Their valuable suggestions have always helped me face the most difficult phases. I have no words to explain their love, care and support. I am really blessed to have them in my life.

Finally on a more personal note, a deep, heartfelt thanks to my in-laws, mother-in-law (Smt Indravati), father-in-law (Sh. Shyam Babu) for their moral support, inspiration and unconditional love without which it would have not possible to complete this work. I am also indebted to my nanaji (Sh. Dwarka Prasad), grandmother in law (Smt. Gayatri Devi), late grandmother and grandfather whose blessings helped me to reach here. I would like to thank my uncles (Sh. Rupendra, Nirmal uncle), aunts (Smt. Santosh and Beena), Devesh, Dhanush, Anshu and Chinu di for their love and care.

My feelings and love for all my friends especially Amarpreet, Mantesh, Pooja, Ashish, Poonam, and Jyoti is inexplicable. I would like to give bottomless thanks to them for their affection and support which was greatly precious for me in my tough time. I am sincerely thankful to all those who have helped me in the successful completion of this work.

I acknowledge the financial support of University Grant Commission, UGC for a fellowship.

Last but not the least, again I thank God who gave me the grace, privilege and opportunity to pursue this program and its successfully completion.

Neha Garg

ABSTRACT

Growing environmental pollution and depleting energy resources are major issues in the present scenario. One of the prime reasons behind the arising environmental pollution is combustion of fossil fuels and their depletion. Therefore, the need of the hour has generated an extensive interest in researchers to develop technologies that provide clean, sustainable, cheap, renewable energy which are also environmentally benign. Electrochemical storage and conversion devices have attracted a great interest to solve these issues. Electrochemical water splitting reaction provides one of the efficient sources of renewable energy (Hydrogen evolution and oxygen evolution). Spinel based mixed transition metal oxides (MTMOs) is important for future energy requirements due to their low cost, high abundance and environmental friendly behavior. Electrocatalytic properties of the functional materials depend on the composition, structure, crystalline phase, and morphology (size and shape). Due to the presence of various cations with more than one oxidation state and unpaired electrons, cobaltite and manganite spinel nanostructures show interesting and highly tunable electrocatalytic properties. Although, various physical and chemical methodologies are known for synthesis of MTMOs, rational design of the efficient electrode material for effective electrochemical technologies is still a challenge.

Motivation of the present thesis is to develop alternate approaches for the synthesis of nanostructured spinel cobaltites and manganites with various morphologies. We focus on the development of an efficient electrocatalyst with controlled size, morphology, composition and structure. Nanostructured electrodes (with high surface/volume ratio, efficient electrochemical activities and cycling performance) have been synthesized using

hydrothermal, microemulsion and coprecipitation methods under ambient conditions. We have investigated various parameters that cooperatively enhance the electrocatalytic efficiency of the material. This thesis deals with the synthesis, characterization and properties of various shapes and size of cobaltites and manganites nanostructures and their properties suitable for electrochemical storage/conversion devices.

In chapter 1, a detailed review of the background literature has been carried out to know the existing research and the major challenges in the area of the available energy source and the materials especially manganites and cobaltites, which are useful for the electrochemical devices. We have also discussed the importance of the nanostructured cobaltites and manganites as efficient electrocatalyst. Although, various high temperature routes, physical and chemical methods known, rational design of the efficient electrode material is still a challenge. So, in this chapter we have discussed the methodologies used for obtaining cobaltites and manganites of controlled size and morphology for efficient electrocatalytic applications.

The controlled synthesis procedure for obtaining NiCo_2O_4 nanorods (assembled from small nanoparticles) with different aspect ratio has been discussed in **chapter 2**. To control the anisotropy of the NiCo_2O_4 nanorods, a surfactant mediated reverse micellar route was used. The effect of surfactants and non-polar phases was studied by varying the chain length of the co-surfactants. Cationic surfactant (CTAB) prefers the alignment of NiCo_2O_4 nanorods with high aspect ratio (~ 12) while non-ionic surfactant (Tergitol) led to the formation of much lower aspect ratio (~ 5) nanorods. We also investigated the electrocatalytic activity of the NiCo_2O_4 nanostructures towards oxygen evolution

reaction. The current work focuses to understand the effect of size of nanostructured electrode towards the electrochemical applications.

In **chapter 3**, we have discussed a template free hydrothermal route for the synthesis of NiCo_2O_4 nanostructures. Different morphologies of NiCo_2O_4 , like square sheets, hexagonal sheets and spheres were synthesized by fine tuning the reaction conditions as well as the selection of the hydrolyzing agents. These synthetic parameters were studied in detail. Shape dependent electrocatalytic study showed significant electrochemical behavior with improved supercapacitance as well as good electrocatalytic properties towards oxygen evolution reaction. Studies showed the enhanced efficiency of NiCo_2O_4 square sheets with enhanced stability.

In **chapter 4**, the role of the surfactant, co-surfactant and non-polar phase during the synthesis of NiMn_2O_4 nanospheres and hexagonal particles using the reverse micellar route are discussed. Slow decomposition of the oxalate precursor (aspect ratio > 3) is the key to maintain the anisotropic morphology of the oxide NiMn_2O_4 nanorods (assembled with smaller nanoparticles). Cationic surfactants lead to anisotropic growth while non-ionic surfactant preferred isotropic growth of nanostructures. The detailed magnetic properties of the above have been studied.

Chapter 5 highlights, the methodology used for the synthesis of novel Mg and Cd based manganites (Mg_2MnO_4 and CdMn_2O_4) under ambient conditions. Mg_2MnO_4 nanorods (assembled from small nanoparticles) have been synthesized using reverse micellar route while CdMn_2O_4 nanocubes have been obtained via a facile co-precipitation route at room temperature. Electrochemical studies showed that Mg_2MnO_4 nanorods act as efficient

electrode towards oxygen evolution reaction and CdMn_2O_4 nanocubes show good anodic behavior towards Li-ion battery applications.

In **chapter 6**, we have discussed composition and phase dependent electrochemical behavior of cobalt manganite nanostructures. The chapter focuses on synthesis of two distinct phases, cubic Co_2MnO_4 and tetragonal CoMn_2O_4 using a simple hydrothermal method without any further annealing. Cubic Co_2MnO_4 nanocubes show efficient electrochemical behavior towards oxygen reduction reaction while tetragonal CoMn_2O_4 nanocubes show better performance towards oxygen evolution reaction (OER) than Co_2MnO_4 .

Conclusions and future prospects of the work carried out are described in **chapter 7**. The thesis has led to the development of low temperature methodologies using co-precipitation, microemulsion route and hydrothermal mediated precursors to obtain various morphologies of nanostructured cobaltites and manganites. Various factors that affect the electrochemical performance have been studied in this thesis and the above study can be extended to a detailed study of the growth controlling parameters for various morphologies of spinel cobaltites and manganites.

TABLE OF CONTENTS

CERTIFICATE		i
ACKNOWLEDGEMENTS		ii
ABSTRACT		v
TABLE OF CONTENTS		ix
LIST OF FIGURES		xvii
LIST OF TABLES		xxix
ABBREVIATIONS AND SYMBOLS		xxxii
CHAPTER 1	Introduction	
1.1	Introduction	2
1.2	Different Methodologies used for Synthesis of Nanomaterials	8
1.2.1	Hydrothermal Method	9
1.2.2	Reverse Micellar Route	11
1.2.2.1	Surfactants	11
1.2.2.2	Co-surfactants	14
1.2.2.3	Importance of Microemulsion Systems	15
1.2.2.4	Formation of Nanoparticles in Reverse Micelles	15
1.2.3	Co-precipitation	17
1.3	Characterization Techniques	18
1.3.1	Powder X-ray Diffraction	18

1.3.1.1	Grain size determination by line broadening studies	19
1.3.2	Thermal Analysis	20
1.3.3	Fourier Transform Infrared Spectroscopy	21
1.3.4	Field Emission Electron Microscopy	22
1.3.5	Transmission Electron Microscopy	23
1.3.6	Energy Dispersive X-ray Analysis (EDAX)/ Energy Dispersive Spectroscopy	26
1.3.7	Brunauer-Emmett-Teller (BET) Surface Area Measurement	26
1.3.8	X-ray Photoelectron Spectroscopy	28
1.4	Properties of Materials	29
1.4.1	Magnetic Properties	29
1.4.2	Electrocatalytic Properties	35
1.4.2.1	Cyclic Voltammetry	37
1.4.2.2	Linear Sweep Voltammetry	39
1.4.2.3	Supercapacitance	40
1.4.2.4	Chronoamperometric Analysis	41
1.5	Challenges and Motivation of the Thesis	41
1.6	References	44

CHAPTER 2 Controlling the Aspect Ratio of NiCo₂O₄ Nanorods for Efficient Electrocatalytic Activity

2.1	Introduction	54
2.2	Experimental	57

2.2.1	Materials and Methods	57
2.3	Characterization Techniques	59
2.3.1	Powder X-ray Diffraction	59
2.3.2	Thermogravimetric Analysis	59
2.3.3	Fourier Transform Infrared Spectroscopy	59
2.3.4	Field Emission Scanning Electron Microscopy	59
2.3.5	Transmission Electron Microscopy	60
2.3.6	X-ray Photoelectron Spectroscopy (XPS)	60
2.3.7	Surface Area Measurement	60
2.3.8	Magnetization Studies	61
2.3.9	Electrochemical Measurements	61
2.3.9.1	Fabrication of Electrode	61
2.4	Results and Discussion	62
2.4.1	Roughness Factor	79
2.5	Conclusions	81
2.6	References	82

CHAPTER 3 Shape Dependent Synthesis of NiCo₂O₄ Nanostructures and their Supercapacitance Behavior

3.1	Introduction	90
3.2	Experimental	93
3.2.1	Materials and Methods	93
3.3	Characterization Techniques	94

3.3.1	Powder X-ray Diffraction	94
3.3.2	Thermogravimetric Analysis	94
3.3.3	Fourier Transform Infrared Spectroscopy	94
3.3.4	Field Emission Scanning Electron Microscopy	95
3.3.5	Transmission Electron Microscopy	95
3.3.6	X-ray Photoelectron Spectroscopy	95
3.3.7	Surface Area Measurement	96
3.3.8	Magnetization Studies	96
3.3.9	Electrochemical Measurements	96
3.4	Results and Discussion	97
3.4.1	Electrochemical Studies	113
3.4.1.1	Cyclic Voltammetry	113
3.4.1.2	Linear Sweep Voltammetry	115
3.4.1.3	Charge-Discharge Studies	117
3.4.1.4	Stability of Electrocatalyst	120
3.5	Conclusions	121
3.6	References	121

CHAPTER 4 Controlling the Morphology of NiMn₂O₄ Nanostructures and their Magnetic Properties

4.1	Introduction	129
4.2	Experimental	131
4.2.1	Materials and Methods	131

4.2.2	Synthesis of the $\text{Ni}_{0.33}\text{Mn}_{0.67}(\text{C}_2\text{O}_4)\cdot 2\text{H}_2\text{O}$ Precursor using a Cationic Surfactant (CTAB)	131
4.2.3	Synthesis of the $\text{Ni}_{0.33}\text{Mn}_{0.67}(\text{C}_2\text{O}_4)\cdot 2\text{H}_2\text{O}$ Precursor using a Non-Ionic Surfactant (Tergitol)	132
4.2.4	Synthesis of the Nickel Manganese Oxide (NiMn_2O_4) from Nickel Manganese Oxalate Precursor Synthesized using CTAB or Tergitol as the Surfactant	133
4.3	Characterization Techniques	133
4.3.1	Powder X-ray Diffraction (PXRD)	133
4.3.2	Thermogravimetric Analysis	133
4.3.3	Fourier Transfer Infrared Spectroscopy	134
4.3.4	Transmission Electron Microscopy	134
4.3.5	Magnetization Studies	134
4.4	Results and Discussion	134
4.5	Conclusions	152
4.6	References	153

**CHAPTER 5 Mg and Cd Based Manganites (Mg_2MnO_4 and CdMn_2O_4)
Nanostructures for Electrocatalytic Applications**

5.1	Introduction	159
5.2	Experimental	162
5.2.1	Material and Methods	162
5.2.1.1	For Mg_2MnO_4	162

5.2.1.2	For CdMn ₂ O ₄	163
5.3	Characterization Techniques	163
5.3.1	Powder X-ray Diffraction	163
5.3.2	Thermogravimetric Analysis	164
5.3.3	Fourier Transform Infrared Spectroscopy	164
5.3.4	Field Emission Scanning Electron Microscopy	164
5.3.5	Transmission Electron Microscopy	164
5.3.6	Elemental EDAX Mapping	165
5.3.7	X-ray Photoelectron Spectroscopy	165
5.3.8	Magnetization Studies	165
5.3.9	Electrochemical Measurements	165
5.3.9.1	Electrode (Mg ₂ MnO ₄) Preparation for Oxygen Evolution Reaction	166
5.3.9.2	Electrode (CdMn ₂ O ₄) Preparation for Lithium Ion Battery Applications	166
5.4	Results and Discussion	167
5.4.1	Results and Discussion for Mg ₂ MnO ₄ Nanostructures	167
5.4.2	Results and Discussion for CdMn ₂ O ₄ Nanostructures	177
5.5	Conclusions	187
5.6	References	188

**CHAPTER 6 Investigation of Electrocatalytic and Magnetic Property of
CoMn₂O₄ and Co₂MnO₄ Nanostructures**

6.1	Introduction	195
6.2	Experimental	197
6.2.1	Materials and Methods	197
6.2.2	Synthesis of CoMn_2O_4 and Co_2MnO_4 Nanostructures	197
6.3	Characterization Techniques	198
6.3.1	Powder X-ray Diffraction	198
6.3.2	Fourier Transform Infrared Spectroscopy	198
6.3.3	Transmission Electron Microscopy	198
6.3.4	Elemental EDAX Mapping	198
6.3.5	X-ray Photoelectron Spectroscopy	199
6.3.6	Surface Area Measurement	199
6.3.7	Magnetization Studies	199
6.3.8	Electrochemical Measurements	200
6.3.8.1	Fabrication of the Electrode for Electrocatalysis	
	Measurement	200
6.3.8.2	Rotating Disk Electrode (RDE) Measurement	200
6.4	Results and Discussion	201
6.5	Conclusions	217
6.6	References	218
CHAPTER 7	Conclusions and Scope for Further Research	223
	Bio-Data of the Author	227

LIST OF FIGURES

Figure No.	Figure Captions	Page No.
Figure 1.1	(a) A complete view of hydrothermal bomb and (b) Commercially available hydrothermal bomb used in the reactions (in our study)	10
Figure 1.2	(a) Schematic diagram of surface active molecule (surfactant) (b) Tergitol (c) Tx-100, (d) CTAB, (e) CPB, (f) AOT	12
Figure 1.3	Schematic diagram of water in oil microemulsion (reverse micelle) droplets	13
Figure 1.4	Mechanism showing the intermicellar exchange of reactants for growing nanocrystals inside microemulsion droplets	16
Figure 1.5	Schematic ray diagram for a transmission electron microscope with the specimen, illuminated with a parallel beam of electrons showing image and diffraction pattern formation by the objective lens and subsequent lenses	25
Figure 1.6	Schematic showing adjacent magnetic dipole moments in (a) Paramagnetic, (b) Ferromagnetic, (c) Antiferromagnetic and (d) Ferrimagnetic material	32
Figure 1.7	Three electrode cell system (Experimental set up)	37
Figure 1.8	(a) Potential against time program for cyclic	38

	voltammetry and (b) A typical cyclic voltammogram for a reversible reaction	
Figure 1.9:	(a) Potential against time program for linear sweep voltammetry and (b) A typical LSV voltammogram	39
Figure 2.1	Flow chart diagram of synthesis of nanomaterials using microemulsion route.	58
Figure 2.2	Powder X-ray diffraction pattern of (a) oxalate precursors and (b) NiCo ₂ O ₄ nanostructures (NCO-1, NCO- 2 and NCO-3)	63
Figure 2.3	Thermogravimetric analysis of oxalate precursor (NCO-1)	64
Figure 2.4	FTIR spectrum of (a) oxalate precursor (b) NiCo ₂ O ₄ nanostructures (NCO-2)	64
Figure 2.5	FESEM images of oxalate precursors (a) NCO-1 (b) NCO-2 (c) NCO-3	65
Figure 2.6	FESEM images of NiCo ₂ O ₄ nanorods synthesized by heating of oxalate precursors at 350 °C, 8h (a) NCO-1 (b) NCO-2(c) NCO-3	66
Figure 2.7	TEM micrographs of oxalate precursors (a) NCO-1 (b) NCO-2 (c) NCO-3	67
Figure 2.8	TEM micrographs of NiCo ₂ O ₄ nanorods synthesized by heating of oxalate precursors at 350 °C, 8h (a) NCO-1 (b) NCO-2 (c) NCO-3	68

Figure 2.9	HR-TEM micrograph of NiCo ₂ O ₄ (a) NCO-1 (b) NCO-2(c) NCO-3	69
Figure 2.10	EDX spectrum of the (a) oxalate precursor (b) NiCo ₂ O ₄ nanorods (NCO-2)	70
Figure 2.11	XPS spectra for NiCo ₂ O ₄ (NCO-2)	71
Figure 2.12	(a) Field dependent magnetic behavior of NiCo ₂ O ₄ nanostructures, (b) FC and ZFC plots of NiCo ₂ O ₄ (NCO-2)	74
Figure 2.13	Cyclic voltammogram of NiCo ₂ O ₄ (NCO-1, 2 and 3) towards oxygen evolution reaction	76
Figure 2.14	Linear sweep voltammogram of NiCo ₂ O ₄ (NCO-1, 2 and 3) towards oxygen evolution reaction	77
Figure 2.15	(a) Chronoamperometric measurement of the NiCo ₂ O ₄ under a bias of 0.8 V vs. Ag/AgCl at pH 14 for 5000 s, (b) TEM of NCO-2 nanorods after electrocatalysis	79
Figure 2.16	(a) Cyclic voltammogram in the double-layer region of the electrode made by the NCO-2 nanorods, at scan rates ranging from 10 to 100 mV s ⁻¹ , (b) Charging current as a function of scan rate for the electrodes of -- Δ- - NCO-2,--□-- NCO-3, and --O-- NCO-1 electrode	80
Figure 3.1	Powder x-ray diffraction pattern of (a) the precursor (mixture of nickel hydroxide and cobalt hydroxide) and (b) NiCo ₂ O ₄ nanostructures synthesized using	98

	hydrolyzing agent as urea (NC-1), NaOH (NC- 2), and NH ₄ OH (NC-3)	
Figure 3.2	Thermogravimetric analysis of the hydroxide precursor synthesized by urea as a hydrolyzing agent	99
Figure 3.3	FT-IR spectra of all the NiCo ₂ O ₄ nanostructures (NC-1, NC-2 and NC-3)	100
Figure 3.4	FESEM micrographs of the hydroxide precursors using (a) urea and (b) NaOH as hydrolyzing agent	101
Figure 3.5	FESEM micrographs of the NiCo ₂ O ₄ nanostructures (a) using urea (b) NaOH and (c) ammonium hydroxide	102
Figure 3.6	FTIR spectra of Ni(NO ₃) ₂ .6H ₂ O and Ni(en) ₃ complexes	103
Figure 3.7	TEM micrographs of the hydroxide precursors obtained using (a) urea (NC-1) (b) ethylenediamine (NC-2)	104
Figure 3.8	TEM micrographs of NiCo ₂ O ₄ nanostructures using (a) urea (NC-1) (b) ethylenediamine (NC-2) and (c) ammonium hydroxide (NC-3)	105
Figure 3.9	HRTEM micrographs of the NiCo ₂ O ₄ nanostructures obtained using (a) urea (NC-1) (b) ethylenediamine (NC-2) and (c) ammonium hydroxide (NC-3)	106
Figure 3.10	Electron diffraction pattern of NiCo ₂ O ₄ nanostructures obtained using (a) urea (NC-1) (b) ethylenediamine (NC-2) and (c) ammonium hydroxide (NC-3)	107
Figure 3.11	EDX spectrum of (a) NC-1, (b) NC-2 and (c) NC-3	108

	nanostructures	
Figure 3.12	Nitrogen adsorption and desorption isotherms measured at 77 K for (a) NC-1, (2) NC-2 and (c) NC-3. The inset shows the corresponding BJH pore size distributions	109
Figure 3.13	XPS spectra of NiCo ₂ O ₄ (NC-1) (a) survey scan, (b) Ni 2p core level, (c) Co 2p core level and (d) O 1s core level	110
Figure 3.14	ZFC and FC plots of NiCo ₂ O ₄ nanostructures using (a) urea (NC-1) (b) ethylenediamine (NC-2) and (c) NH ₄ OH (NC-3)	111
Figure 3.15	Field-dependent magnetic behavior of (1) (a) NC-I, (b) NC-II, and (c) NC-III at (a) 5 K and (2) at 300 K. Insets: corresponding magnetization data of sample NC-III at an enhanced scale	112
Figure 3.16	(a). Cyclic voltammogram of NiCo ₂ O ₄ nanostructures (NC-1, NC-2 and NC-3) as catalyst for oxygen evolution reaction, (b) Plot of current density vs. scan rate	115
Figure 3.17	Linear sweep voltammogram of NiCo ₂ O ₄ (NC-1, 2 and 3) during oxygen evolution reaction	116
Figure 3.18	(a) Charge-discharge curves at different current	118

	densities of NC-1 electrode; (b) Galvanostatic charge-discharge at a current density of 0.1 A g ⁻¹ for the three electrodes (NC-1, NC-2 & NC-3) (c) Variation of specific capacitance with cycle number at 12 A g ⁻¹ of the NC-1 (square sheet) electrode.	
Figure 3.19	(a) Chronoamperometric measurement of the NiCo ₂ O ₄ under a bias of 0.6 V vs Ag/AgCl for 5000 s, (b) TEM of NC-1 (square sheets) after electrocatalysis (Chronoamperometric measurement for 5000 s) (inset shows HR-TEM of NC-1)	120
Figure 4.1	Powder x-ray diffraction pattern of nickel manganese oxalate Ni _{0.33} Mn _{0.67} (C ₂ O ₄).2H ₂ O using (a) surfactant less route (b) CTAB / isooctane / 1-butanol / aq. (c) CTAB / cyclohexane / 1-butanol / aq. (d) Tergitol / cyclohexane / 1-butanol / aq. (e) Tergitol / cyclohexane / 1-hexanol or 1-octanol(f) / aq.	135
Figure 4.2	Thermogravimetric analysis of nickel manganese oxalate precursor obtained using Tergitol/cyclohexane/1-butanol/aq. microemulsions	136
Figure 4.3	Powder X-ray diffraction pattern of nickel manganese oxide NiMn ₂ O ₄ obtained at 800 °C from oxalate precursors	137
Figure 4.4	FTIR of (a) nickel-manganese oxalate precursor and	140

	(b) NiMn ₂ O ₄	
Figure 4.5	TEM micrograph of nickel manganese oxalate Ni _{0.33} Mn _{0.67} (C ₂ O ₄).2H ₂ O obtained using microemulsion system of (a) surfactant less route (b) CTAB / isooctane / 1-butanol / aq. (c) CTAB / cyclohexane / 1-butanol / aq. (d) Tergitol / cyclohexane / 1-butanol / aq. (e) Tergitol / cyclohexane / 1-hexanol / aq. and Tergitol /cyclohexane /1-octanol/aq.	142
Figure 4.6	TEM micrograph of nickel manganese oxide obtained after calcination of Ni _{0.33} Mn _{0.67} (C ₂ O ₄).2H ₂ O at 800 °C obtained using microemulsion system of (a) surfactant less route (b) CTAB / isooctane / 1-butanol / aq. (c) CTAB / cyclohexane / 1-butanol / aq. (d) Tergitol / cyclohexane / 1-butanol / aq. (e) Tergitol / cyclohexane / 1-hexanol / aq. and Tergitol /cyclohexane /1-octanol/aq.	145
Figure 4.7	HRTEM micrograph of nickel manganese oxide obtained from Ni _{0.33} Mn _{0.67} (C ₂ O ₄).2H ₂ O at 800 °C using microemulsion system of (a) surfactant less route (b) CTAB / isooctane / 1-butanol / aq. (c) CTAB / cyclohexane / 1-butanol / aq. (d) Tergitol / cyclohexane / 1-butanol / aq. (e) Tergitol / cyclohexane / 1-hexanol / aq. and Tergitol /cyclohexane /1-octanol/aq.	147

Figure 4.8	χ_m vs. T plot of pure NiMn_2O_4 obtained from $\text{Ni}_{0.33}\text{Mn}_{0.67}(\text{C}_2\text{O}_4) \cdot 2\text{H}_2\text{O}$ at 800 °C using microemulsion system of (a) surfactant less route (b) CTAB / isooctane / 1-butanol / aq. (c) CTAB / cyclohexane / 1-butanol / aq. (d) Tergitol / cyclohexane / 1-butanol / aq. (e) Tergitol / cyclohexane / 1-hexanol / aq. and Tergitol /cyclohexane /1-octanol/aq.	148
Figure 4.9	Variation of χ_m with different size and morphologies of NiMn_2O_4 obtained from (a) surfactant less route (b) CTAB / isooctane / 1-butanol / aq. (c) CTAB / cyclohexane / 1-butanol / aq. (d) Tergitol / cyclohexane / 1-butanol / aq. (e) Tergitol / cyclohexane / 1-hexanol / aq. and Tergitol /cyclohexane /1-octanol/aq.	149
Figure 4.10	Variation of T_c with different size and morphologies of NiMn_2O_4 obtained from (a) surfactant less route (b) CTAB / isooctane / 1-butanol / aq. (c) CTAB / cyclohexane / 1-butanol / aq. (d) Tergitol / cyclohexane / 1-butanol / aq. (e) Tergitol / cyclohexane / 1-hexanol / aq. and Tergitol /cyclohexane /1-octanol/aq.	150
Figure 4.11	M-H plot of pure NiMn_2O_4 obtained at 800 °C $\text{Ni}_{0.33}\text{Mn}_{0.67}(\text{C}_2\text{O}_4) \cdot 2\text{H}_2\text{O}$ obtained using microemulsion system of (a) surfactant less route (b) CTAB / isooctane / 1-butanol / aq. (c) CTAB / cyclohexane / 1-	151

	butanol / aq. (d) Tergitol / cyclohexane / 1-butanol / aq. (e) Tergitol / cyclohexane / 1-hexanol / aq. and Tergitol /cyclohexane /1-octanol/aq.	
Figure 5.1	Powder X-ray diffraction pattern of magnesium manganese oxalate $Mg_{0.67}Mn_{0.33}(C_2O_4).2H_2O$ precursor	167
Figure 5.2	Thermogravimetric analysis of magnesium manganese oxalate precursor	168
Figure 5.3	Powder X-Ray diffraction pattern of Mg_2MnO_4 obtained at (a) 500 °C (b) different temperatures (1) 500 °C (2) 600 °C, (3) 700 °C and (4) 800 °C	169
Figure 5.4	FT-IR spectrum of (a) magnesium manganese oxalate precursor and (b) Mg_2MnO_4	170
Figure 5.5	TEM images of oxalate precursor $Mg_{0.67}Mn_{0.33}(C_2O_4).2H_2O$	170
Figure 5.6	(a) TEM images of the Mg_2MnO_4 and (b) HRTEM micrographs of Mg_2MnO_4	171
Figure 5.7	TEM of the Mg_2MnO_4 calcined at different temperature (a) 600 °C, (b) 700 °C and (c) 800 °C	172
Figure 5.8	FESEM images of Mg_2MnO_4 at (a) 500 °C, (b) 600 °C, (c) 700 °C and (d) 800 °C	173
Figure 5.9	EDX spectra of (a) oxalate precursor and (b) Mg_2MnO_4	173
Figure 5.10	Magnetic and inverse magnetic susceptibility vs.	174

	temperature plot of Mg_2MnO_4 obtained at 500 °C	
Figure 5.11	Cyclic voltammogram of Mg_2MnO_4 obtained at 500 °C in 1 M KOH and (b) stability curve for 30 cycles	175
Figure 5.12	PXRD pattern of CdMn_2O_4 using (a) PVP (CM-P) and (b) without PVP (CM-N)	178
Figure 5.13	FT-IR spectrum of CdMn_2O_4 (a) CM-N and (b) CM-P	179
Figure 5.14	TEM images of CdMn_2O_4 nanostructures (a) using PVP (CM-P) and (b) without using PVP (CM-N)	180
Figure 5.15	HRTEM images of CdMn_2O_4 nanostructures (a) without using PVP and (b) with PVP	180
Figure 5.16	Elemental EDX mapping of CdMn_2O_4 (a) CM-N and (b) CM-P	181
Figure 5.17	EDX spectrum of CdMn_2O_4 (a) CM-N, and (b) CM-P nanostructures	182
Figure 5.18	Nitrogen adsorption and desorption isotherms measured at 77 K for CdMn_2O_4 (a) CM-N and (b) CM-P	183
Figure 5.19	XPS spectra of Mn 2p core level of (a) CM-N and (b) CM-P	184
Figure 5.20	(a) Magnetic and inverse magnetic susceptibility vs. temperature plot of CdMn_2O_4 and (b) linear fit curve of $1/\chi$ vs. T (to calculate θ)	185
Figure 5.21	(a) The first discharge and charge curves of CdMn_2O_4	186

	(CM-N and CM-P) and (b) cycling performance of CdMn_2O_4 at the current density of 38 mA g^{-1}	
Figure 6.1	Powder x-ray diffraction of (a) CoMn_2O_4 and (b) Co_2MnO_4 nanostructures	202
Figure 6.2	FTIR spectra of CoMn_2O_4 and Co_2MnO_4 nanostructures	202
Figure 6.3	Transmission electron microscope of CoMn_2O_4 and Co_2MnO_4 nanostructures	203
Figure 6.4	HRTEM images of (a) CoMn_2O_4 and (b) Co_2MnO_4 nanostructures	203
Figure 6.5	Elemental EDX mapping of (a) CoMn_2O_4 and (b) Co_2MnO_4 nanostructures	204
Figure 6.6	TEM-EDX of (a) CoMn_2O_4 and (b) Co_2MnO_4 nanostructures	205
Figure 6.7	Survey spectrum for both the (a) CoMn_2O_4 and (b) Co_2MnO_4 nanocubes	205
Figure 6.8	XPS spectra of CoMn_2O_4 (a) Co2p core level, (b) Mn 2p core level, and (e) O 1s core level and of Co_2MnO_4 (c) Co 2p core level, (d) Mn 2p core level, and (f) O 1s core level respectively	206
Figure 6.9	Nitrogen adsorption and desorption isotherms measured at 77 K for (a) CoMn_2O_4 and (b) Co_2MnO_4 nanocubes	207

Figure 6.10	The temperature dependence of magnetization measured in ZFC and FC processes with an applied field of 500 Oe	208
Figure 6.11	M vs. H plot of (a) CoMn_2O_4 and (b) Co_2MnO_4 nanocubes at 7 T	209
Figure 6.12	Electrochemical application of nanocrystalline CoMn_2O_4 and Co_2MnO_4 as ORR electrocatalyst (a) Linear sweep voltammogram of the ORR using catalyst-modified RDEs in O_2 -saturated alkaline electrolyte at 400 rpm (b) Rotation-speed dependent current-potential curves recorded on Co_2MnO_4 electrodes in O_2 -saturated 1 M KOH solution and (c) the corresponding K-L curve (d) Chronoamperometry curves of the ORR for Co_2MnO_4 nanocubes obtained at -0.45 V in oxygen-saturated 0.1 M KOH under constant rotating (400 rpm)	211
Figure 6.13	(a) Cyclic voltammogram of the OER in 1 M KOH electrolyte (b) Stability curve of CoMn_2O_4 nanostructures for 25 cycles	214

LIST OF TABLES

S. No.	Title	Page No.
Table 2.1	Magnetic properties of NiCo ₂ O ₄ nanorods obtained after decomposing the oxalate precursor	73
Table 2.2	Electrocatalytic properties of NiCo ₂ O ₄ nanorods as electrocatalyst towards oxygen evolution reaction	78
Table 3.1	Magnetization, Remanent magnetization and coercive field of NiCo ₂ O ₄ nanostructures (NC-1, NC-2 and NC-3)	113
Table 3.2	Electrocatalytic properties of NiCo ₂ O ₄ nanostructures as electrocatalyst towards the oxygen evolution reaction (OER)	117
Table 3.3	Specific capacitance of NC-1 at various current densities	119
Table 4.1	Compositional analysis by AAS and TEM-EDX studies of nickel manganese oxalate precursor and nickel manganese oxides (digit in bracket indicates the standard deviation calculated from repetitions of the same experiment for six sets)	138
Table 4.2	Zeta potential studies of nickel manganese oxalate	143
Table 6.1	Magnetic analysis of CoMn ₂ O ₄ and Co ₂ MnO ₄ nanostructures	209
Table 6.2	Percentage analysis of the Co and Mn ions in	215

	CoMn ₂ O ₄ and Co ₂ MnO ₄ nanostructures	
Table 6.3	Percentage calculation of oxygen ions in both CoMn ₂ O ₄ and Co ₂ MnO ₄ nanostructures	217

Abbreviations and Symbols

Å	Angstroms
°C	Centigrade
µm	Micrometer
nm	Nanometer
T	Temperature
T _N	Neel Temperature
T _c	Curie Temperature
τ _N	Néel Relaxation Time
T _B	Blocking Temperature
K	Kelvin
°	Degree
Hz	Hertz
2θ	Two Theta
λ	Wavelength
cP	Centipoise
eV	Electron volt
ECs	Electrochemical Capacitors
LIBs	Lithium-ion Batteries
MOBs	Metal Oxide Batteries
FCs	Fuel Cells
RM	Reverse Micelle

MTMOs Mixed Transition Metal Oxides

CTAB Cetyltrimethylammonium bromide

XRD X-ray Diffraction

PXRD Powder X-ray Diffraction

TGA Thermogravimetric Analysis

DTA Differential Thermal Analysis

FT IR Fourier Transform Infrared Spectroscopy

FESEM Field Emission Scanning Electron Microscopy

TEM Transmission Electron Microscopy

HRTEM High Resolution Transmission Electron Microscopy

ED Electron diffraction

EDAX Energy Dispersive X-ray Analysis

BET Brunauer-Emmett-Teller

XPS X-ray Photoelectron Spectroscopy

CV Cyclic Voltammetry

LSV Linear Sweep Voltammetry

μ Magnetic Moment

H Magnetic Field

μ_B Bohr-Magneton

M Magnetization

χ_m Molar Magnetic Susceptibility

χ_m^{-1} Inverse Molar Magnetic Susceptibility

M_s Saturation Magnetization

Mr	Remnant Magnetization
Oe	Oersted
emu	Electromagnetic Unit
vs.	Versus
J	Current Density
H	Applied Field
eq.	Equation
°C	Centigrade
μm	Micrometer
nm	Nanometer
mm	Millimetres
min	Minutes
h	Hours
s	Seconds
NHE	Normal Hydrogen Electrode
HER	Hydrogen Evolution Reaction
OER	Oxygen Evolution Reaction